

Jean-Paul Montagner and Laurent Guillot

*Seismological Laboratory, CNRS URA 195
Institut de Physique du Globe, Paris, France*

color versions of the respective figures in the text.

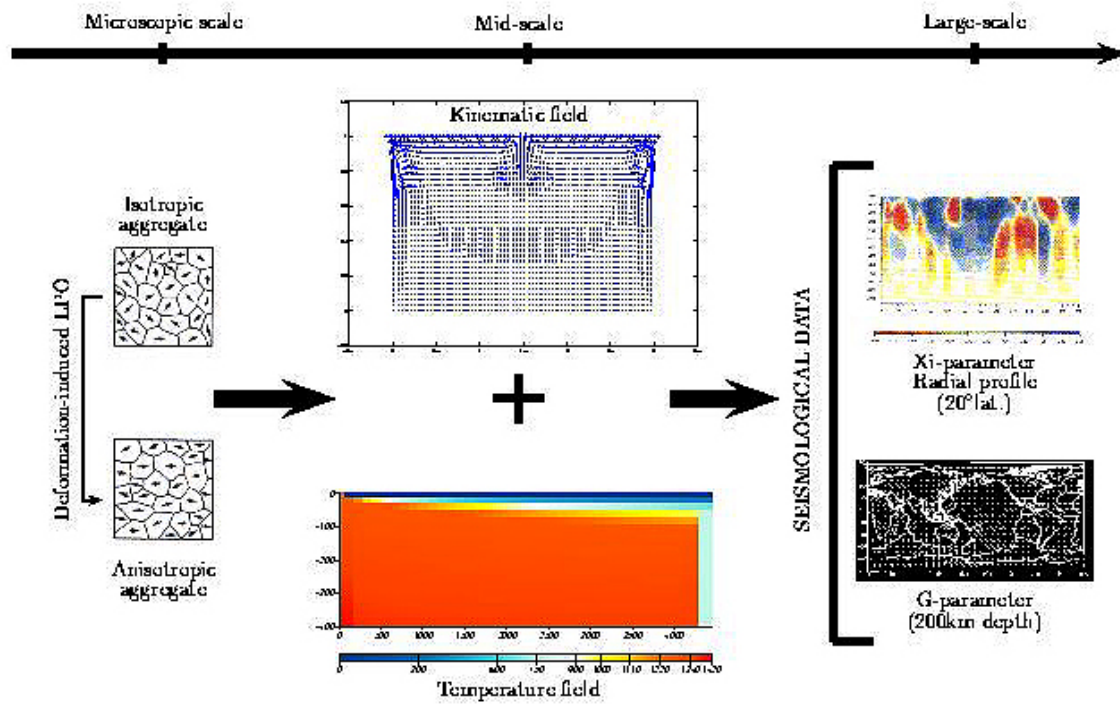


Figure 2. Different steps from mineralogical anisotropy at microscopic scale to observable seismic anisotropy at large scale.

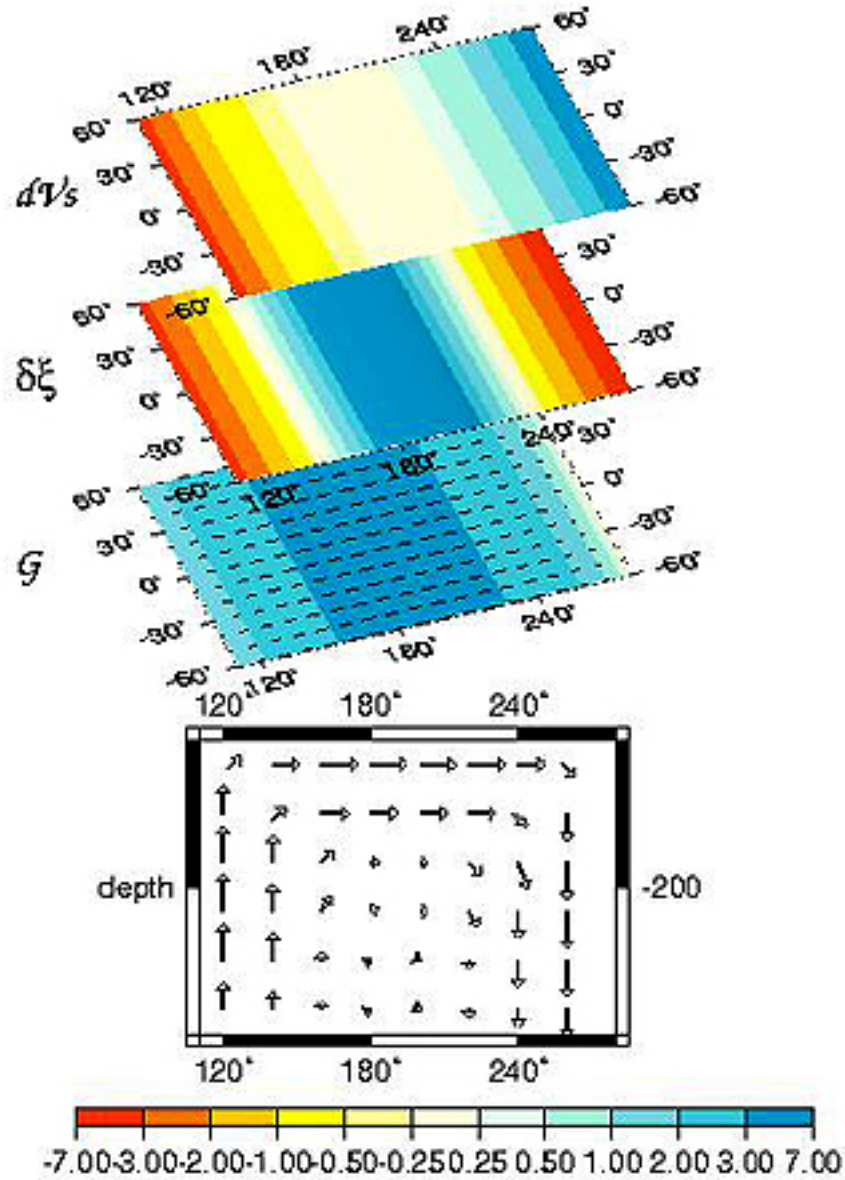


Figure 5. The seismic observable parameters V_S , ξ , G , ψ_G associated with a simple convecting cell in the upper mantle, assuming lattice-preferred orientation of anisotropic minerals such as olivine. A vertical flow is characterized by a negative ξ radial anisotropy (ratio between V_{SH} and V_{SV}) and a small azimuthal anisotropy ($G \approx 0$). An upwelling (resp. downwelling) is characterized by a large positive (resp. negative) temperature anomaly inducing $\delta V_S < 0$ (resp. $\delta V_S > 0$). A predominant large-scale horizontal flow will be translated into a significant amplitude of the G azimuthal anisotropy and its orientation will reflect the direction of flow (with a 180° ambiguity).

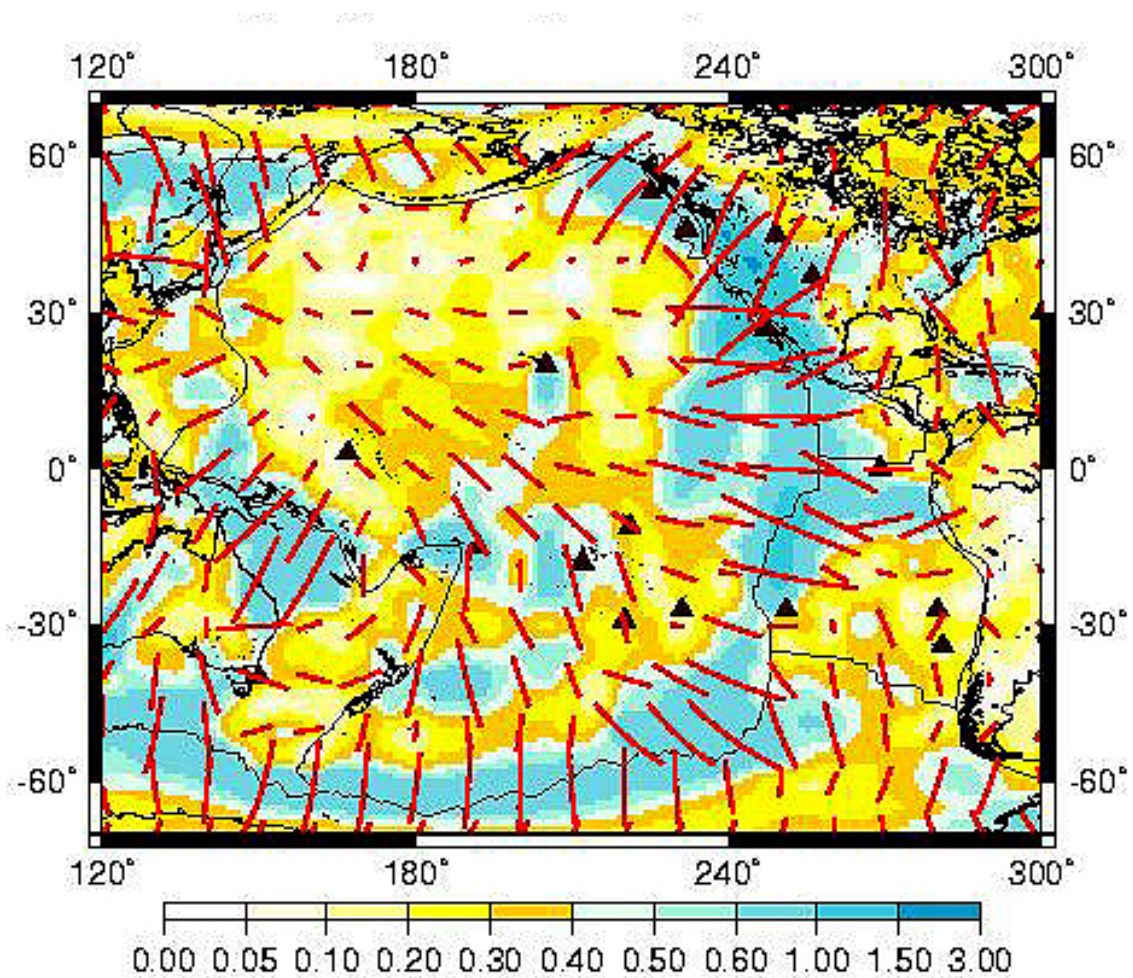


Figure 6. Distributions of synthetic delay time δt_{SKS}^{max} and azimuth Ψ_{SKS} at the surface of the Earth, such as derived from the anisotropic tomographic model of Montagner (2002), derived from data of Ekström and Dziewonski 1998). The crustal part of the 3SMAC -model (Ricard et al. 1996) has been removed. The synthetic map of SKS is calculated by using the method of Montagner et al. (2000), from the G-distribution of V_{SV} azimuthal anisotropy. The length of lines is proportional to δt_{SKS} .

Fig 8: V_{SV} 024PS1 Inv ACY400 (3SMAC corr)

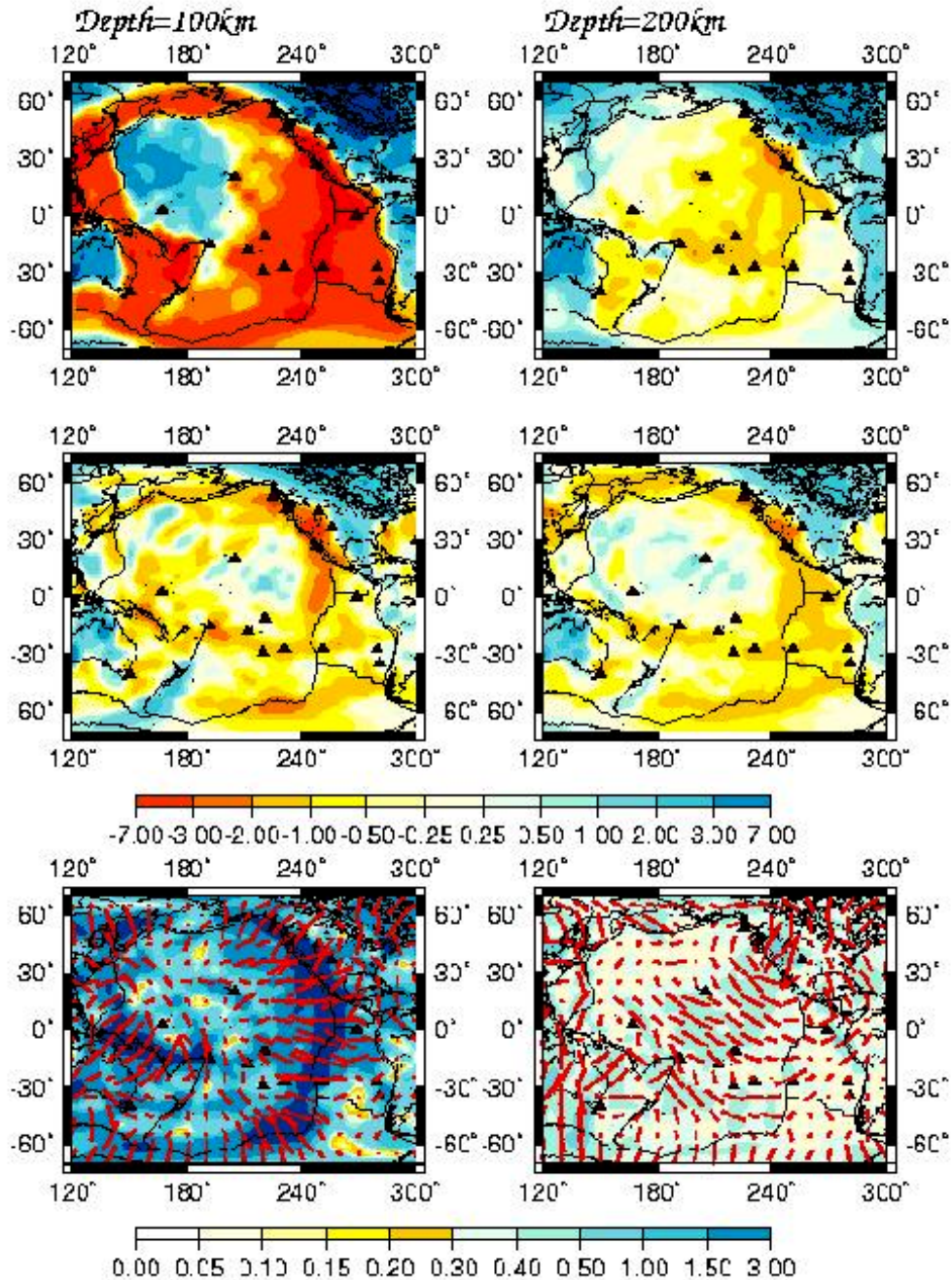


Figure 8. Result of the simultaneous inversion of Rayleigh and Love waves dispersion and their azimuthal variations at 100 km depth (left) and 200 km depth (right). (adapted from Montagner 2002). (Top): Distribution of the V_{SV} parameter in %. (Middle): ξ distributions in % with respect to ACY400 (Montagner and Anderson 1989b). Be aware that ξ anomalies are plotted with respect to a reference value different from 0. (Bottom): Anisotropy map of the G-parameter (V_{SV} azimuthal anisotropy).

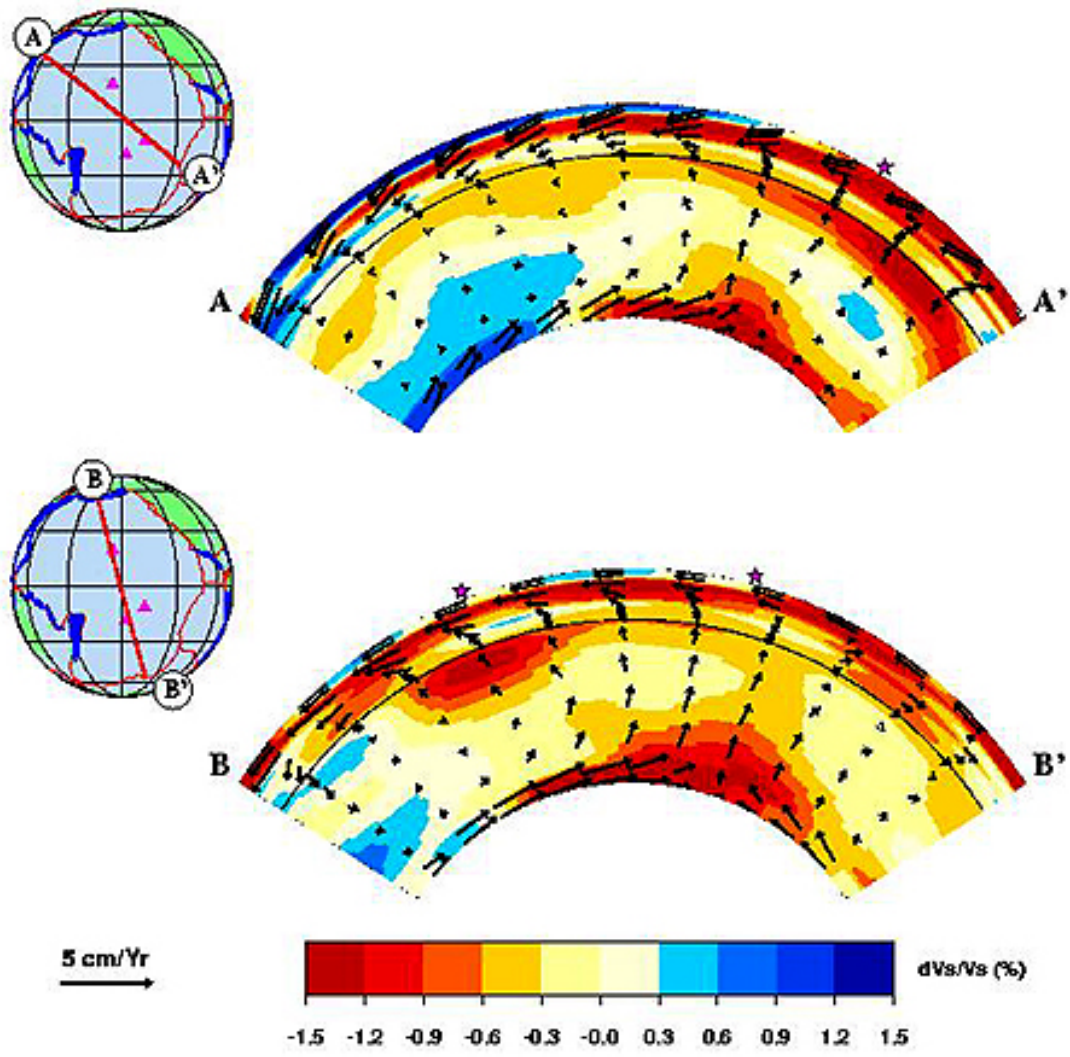


Figure 9. Two whole mantle cross-sections through the Ekstrom and Dziewonski tomographic model (1998) along great circles. Also shown in the inset maps are triangles which represent the locations of 3 Pacific hotspots. The superimposed black arrows in the cross-sections represent the mantle flow velocities predicted on the basis of the buoyancy forces derived from shear velocity anomalies. (Adapted from Gaboret et al. 2002).

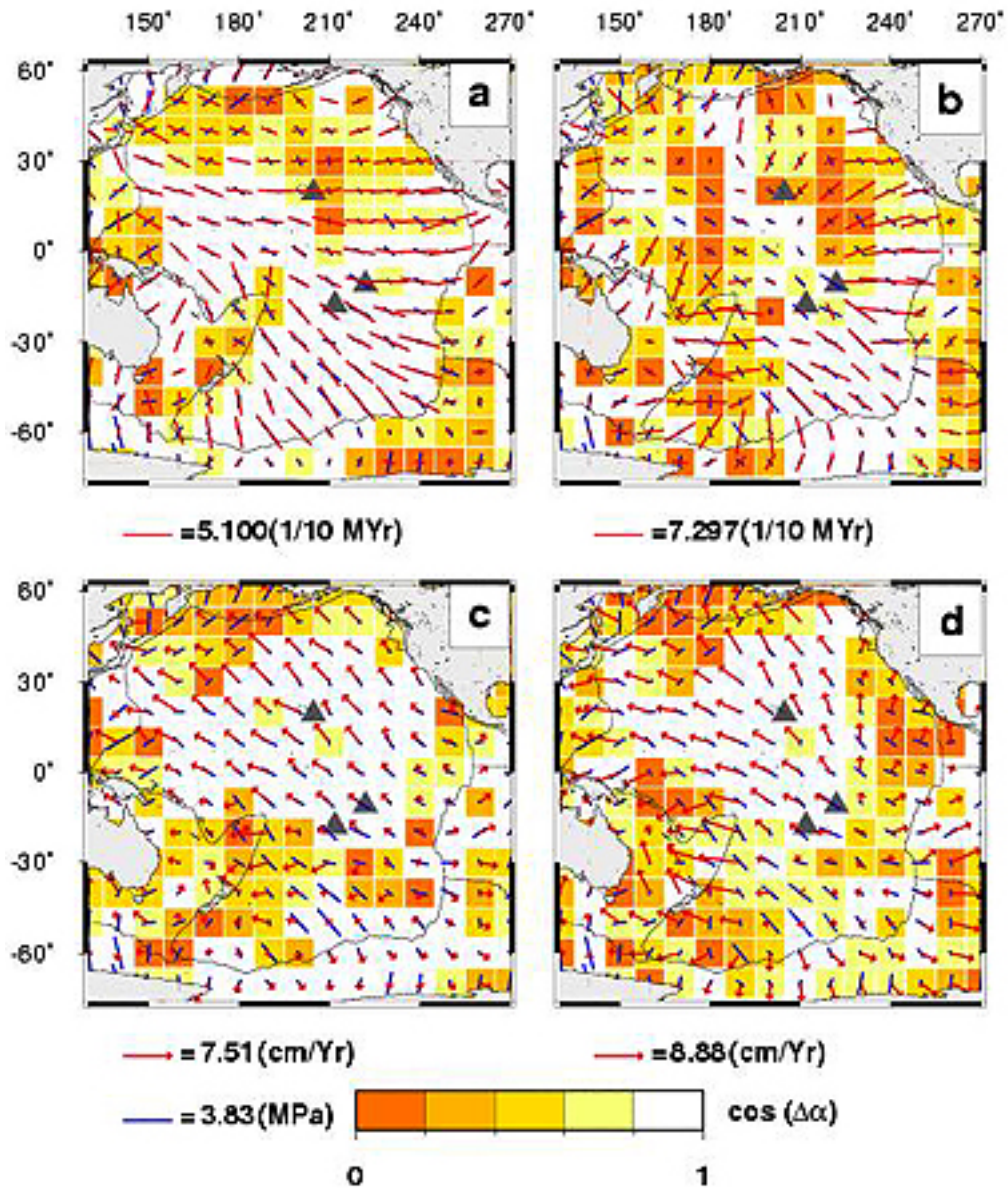


Figure 10. Comparison of Azimuthal seismic anisotropy and the direction of maximum stretching predicted by the flow model presented in Figure 9. (Adapted from Gaboret et al. 2002).